Atomistic simulation of Ag thin films on MgO(100) substrate: A template substrate for heterogeneous adsorption

A. Ouahab and C. Mottet*
CRMCN-CNRS, Campus de Luminy, case 913, 13288 Marseille Cedex 9, France

J. Goniakowski
INSP, Campus de Boucicaut, 140 Rue de Lourmel, 75015 Paris, France
(Received 10 January 2005; revised manuscript received 6 April 2005; published 8 July 2005)

The nanostructuration of Ag thin films deposited on the MgO(100) substrate is simulated by classical molecular dynamics using a tight-binding many-body potential for the metal-metal bonds and a potential fitted to *ab initio* calculations for the metal–oxide ones. Due to the lattice mismatch between the Ag deposit and the MgO(100) substrate, the silver film is strained. The stress is partially released by the introduction of misfit dislocations at the interface. These dislocations form a network with a periodicity of about 10 nm, which varies for ultrathin films according to the film thickness. The strain induced by the interfacial dislocation cores propagates across the silver film up to the surface driving to the nanostructuration of the surface. The atomistic results are compared to the predictions of the elasticity theory. The theoretical results are in a nice agreement with recent experiments obtained by grazing incidence small angle x-ray scattering revealing a self-organization of Co clusters adsorbed on a thin film of Ag/MgO(100) [F. Leroy, G. Renaud, A. Letoublon, R. Lazzari, C. Mottet and J. Goniakowski (unpublished)]. We show that the preferential Co adsorption site is obtained on top of tensile surface sites and that the periodicity of the clusters' self-organization can be tuned by the Ag film thickness.

DOI: 10.1103/PhysRevB.72.035421 PACS number(s): 68.55.−a, 68.47.Jn, 68.43.Bc

I. INTRODUCTION

Nanostructuration of surfaces used as templates for the self-organized growth of clusters is a subject of intensive research. The aim is to achieve ordered, homogeneous size and shape, and high density clusters. Such a collection of nanoclusters can present very interesting properties, either in microelectronics as quantum dots,[2] or in magnetism[3] and also in catalysis.[4] The self-organization and homogeneity of the clusters' distribution result from the nanostructuration of the substrate due to long-range interactions that extend far beyond the range of typical interatomic interactions.[5] Many observations of self-organization have been reported concerning a large variety of systems. Among them, we can distinguish pure surfaces involving surface reconstruction,[6,7] heteroepitaxial systems driving to misfit dislocations networks,[8,9] chemisorption on metallic surface,[10] or both of the two last processes involved in the same system.[5] There have been a lot of studies on the (111)-oriented lattice-mismatch heterogeneous metallic systems. Moiré superstructures have been predicted theoretically on the Ag/Cu(111) system[11] before to be experimentally observed on various systems, such as Ag/Pt(111),[12] Au/Ni(111),[13] and Ag/Cu(111).[8,14,15] In the last two cases, triangle dislocation loops in the underlying substrate surface were observed by scanning tunneling microscope and confirmed by atomistic simulations as a possible alternative to relax the stress induced by the misfit. In any case, the periodic variation of the strain/stress area due to such superstructures leads to a variation of adatom binding energy and makes them feasible candidates for island nucleation network.[16]

Strain-relief patterns induced by misfit dislocation networks are mostly observed on metallic[16,17] and semiconductor[18,19] systems, but usually less in metal–oxide ones.[20] An Ag–MgO(100) interface, is a model system that has given rise to a large number of theoretical[21–30] and experimental studies.[31–37] It is now well established, from extended x-ray-absorption fine structure analysis[32] and grazing-incidence x-ray-scattering (GIXS) and grazing-incidence small-angle x-ray scattering (GISAXS) experiments[33–35] that the epitaxial growth follows the cube-on-cube epitaxy with respect to MgO(100) with preferential adsorption of Ag atoms on top of oxygen sites, in agreement with most of the theoretical studies.[23–25,27] Moreover, the GIXS have shown that the lattice mismatch leads to a misfit dislocation network with interfacial misfit dislocations oriented along the ⟨110⟩ direction.[33,35] Even in such a case of particularly small misfit (3%), we will see using atomistic simulations that the residual strain stored in the Ag layer, after the formation of interfacial misfit dislocations, leads to a nanostructuration of the Ag free surface. Such a surface strain field modulation due to the buried incoherent interface has been described in the framework of the elasticity theory.[38,39] It is notably found that for a lattice-mismatch heterogeneous system with misfit $f=(a_{\mathrm{subs}}-a_{\mathrm{layer}})/a_{\mathrm{layer}}$ and interfacial dislocation network of period $\Lambda=b/f$, where b is the Burger's vector amplitude, a periodic strain field is created at the free surface which varies as h^{-1} in the vicinity of the core dislocation (film thickness $h \ll \Lambda$) and as $h\exp(-h)$ for $h > \Lambda$. In the present study, we will compare quantitatively the atomistic results with the predictions of the classical theory of elasticity following the development proposed by Bonnet and Verger-Gaugry[38], Bourret[39] and Willis *et al.* [40]

The smaller the misfit (3%), the larger the interfacial dislocation network (about 10 nm square in the ⟨110⟩ direction),

so that the atomistic description of the Ag/MgO(100) interface involves a large number of atoms (about 1000 atoms in each plan), as well as a complex set of inhomogeneous atomic relaxations. This disables the direct use of *ab initio* methods which are the best ones to take into account the precise electronic structure and energetics of the system. Instead, we propose a many-body approach which couples a many-body potential based on the second-moment approximation (SMA) for metal–metal interactions and a many-body potential energy surface (PES) fitted to *ab initio* calculations for the metal–oxide interaction.[41] Indeed, whereas many-body potential is widely used in metallic systems, so far there is no reliable potential able to take into account the electronic nature of metal–oxide interactions. First-principles calculations based on the density functional theory (DFT) in the generalized gradient approximation (GGA) have proved to be reliable in the prediction of the preferential adsorption site (oxygen sites) and in a correct estimation of principle features of adsorption energetic.[42]

Static and dynamical properties are studied in microcanonical or canonical ensemble using molecular dynamics with a quenched procedure (microcanonical) to find the energy minimum at 0 K and at finite constant temperature (canonical) to display a dynamical effect in order to better compare with experimental results.

The paper is organized as follows: The energetic model together with the simulation method and elasticity theory elements are described in Sec. II; the results on the Ag film patterning are presented in Sec. III, and the results of Co preferential nucleation in Sec. IV. Conclusions are given in last section.

II. THE MODEL

A. Atomistic approach

The energetic model couples a tight-binding SMA potential for metal–metal interactions and a PES approach fitted to *ab initio* results for metal–oxide interactions.

The SMA many-body potential proposed by Rosato, *et al.*[43] is a many-body potential comparable to the well-known embedded atom method developed by Daw and Baskes.[44] Here, the attractive part of the cohesion energy is derived analytically from the band energy in the framework of the tight-binding model, assuming a rectangular density of states fitted to the second moment of the actual density of states. Such a model is particularly well suited to model transition and noble metals where the cohesion is governed by the *d* electrons band.[45] The attractive many-body term coming from the band energy for an atom at site n is given by

$$E_n^b = -\left\{ \sum_{m, r_{nm} < r_c} \xi^2 \exp\left[-2q\left(\frac{r_{nm}}{r_0} - 1 \right) \right] \right\}^{1/2}. \quad (1)$$

The stability of the system is ensured by adding a phenomenological core-repulsion term of the Born–Mayer type:

TABLE I. Parameters of the SMA potential.

Metal	ξ(eV)	A(eV)	q	p
Ag	1.19402	0.10433	3.190	10.790
Co	1.84297	0.17569	2.975	9.210
Ag–Co	1.47756	0.14436	3.085	10.001

$$E_n^r = \sum_{m, r_{nm} < r_c} A \exp\left[-p\left(\frac{r_{nm}}{r_0} - 1 \right) \right]. \quad (2)$$

and $E_n^{\mathrm{Met}} = E_n^b + E_n^r$. In these expressions, r_{nm} is the distance between atoms n and m, r_c is the cutoff radius of the interactions (in the following calculations, we use the above form of the potential up to the second-neighbor distance, and smoothly link the potential to zero at the third-neighbor distance), and r_0 is the first-neighbor distance. The parameters ξ, q, A, and p are fitted on bulk cohesive energy,[46] lattice parameter and elastic constants.[47] They are given in Table I.

There is no simple and reliable semiempirical potential of the same type as the one described just before for the metal–oxide interaction. First-principle calculations based on the DFT have been used in order to better characterize the electronic structure and thus the energetics of the Ag/MgO(100) interface.[23–27] In light of these studies, we know that the interaction is rather weak (physisorption type), with a weak charge transfer (less than 0.1 electron) and with a preferential adsorption on top of the oxygen atoms. As the quantitative values do not always converge between the different methods (Hartree–Fock approach,[24,26,27] local density approximation (LDA),[23,25] and generalized gradiant approximation GGA)[25] we performed systematic DFT calculations in the frame of full potential-linear augmented plane wave (FP-LAPW)(Ref. 48) scheme with the LDA and GGA treatment. As the GGA is better suited to describe the separated materials, we choose it for the interface. The potential has been fitted on a series of model pseudomorphic structures (0.25, 1, and 5 ML) varying the adsorption site (on top of the oxygen atom, on top of the magnesium atom or in the hollow sites) as a function of the separation distance between the Ag and MgO surfaces. The corresponding curves are displayed in Fig. 1. The adhesion energy for the perfect pseudomorphic interface is 0.26 eV/atoms=0.46 J/m^2. The analytical form of the potential energy surface has been described in Ref. 41. It counts 27 different parameters listed in Ref. 49. The interaction of the metal with the MgO support is limited to the first monolayer of the metal in contact with the oxide. The adhesion energy varies in the range from 0.05 to 0.45 eV/atoms depending on the adsorption site and metal coverage, respectively, for one or more monolayers adsorbed on top of Mg atoms and 0.25 of monolayer adsorbed on top of the O atoms. The interfacial distance ranging, respectively, from 3.39 to 2.46 Å. The Ag/MgO(100) interface energy presents the particularity to evolve not monotonically with the coverage as in the case of Pd/MgO(100).[42] Indeed, a minimum binding energy is obtained for the deposition of one monolayer on top of oxygen, but the energy difference is rather small and could be at the limit of the accuracy of the

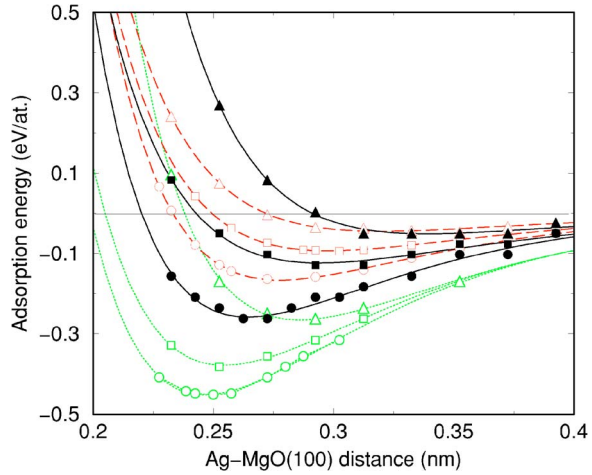

FIG. 1. (Color online) Adsorption energy of Ag deposited on MgO(100): The points represent the DFT-LAPW calculations, the curves represent the analytical form of the PES. Full, dashed, and dot-dashed lines represent, respectively, 5, 1, and 0.25 monolayer Ag coverages, whereas circle, triangle, and square represents the adsorption on top of oxygen, magnesium, and hollow sites.

DFT approximation for that system. Anyway, in the following, we will consider only silver layers of more than one monolayer, i.e., a coordination $Z \geqslant 8$.

Finally, the total energy on N metal atoms is the sum of the contributions of the metal–metal and metal–oxide interactions :

$$E_{\mathrm{tot}} = \sum_{n=1}^{N} E_n^{\mathrm{Met}} + E_n^{\mathrm{Met-MgO}}. \tag{3}$$

There are three remarks on the model.

First, although the two contributions are simply added as in a pairwise interaction model, the many-body effects induced by the adsorption on the oxide are taken into account effectively by the Z-dependent fit to the *ab initio* adsorption energies.

Second, the molecular dynamics simulations are performed on metal atoms whereas the oxide surface is frozen. The approximation of a frozen MgO surface comes from experimental observations of very small atomic relaxation in the MgO(100) substrate[34] and has already been justified in the case of larger misfit interfaces.[41] However, the case of three-dimensional (3D) growth and two-dimensional (2D) interface is evidently different since the interfacial area in the first case represents only a fractional part of the total interface area of the second case. It is to be noted that contrary to homogeneous metallic or semiconducting interfaces, the heterogeneous metal–oxide interface is a particular case where the elastic tetragonal distortion induced by the misfit costs less energy in the metal than in the oxide part.[50]

Third, it has to be noted that in the DFT calculations, the MgO lattice parameter is optimized with the value of 4.25 Å. However, in order to reproduce the experimental misfit of the Ag/MgO system (3%), we take the experimental value (4.21 Å) in the atomistic simulations.

Quenched molecular dynamics is performed in the microcanonic ensemble in order to look for the minimum energy superstructures at the interface and to analyze the local atomic stress σ_n at site n in the silver layer. The atomic stress is given by the trace of the stress tensor σ_{ij} equal to the opposite of the isostatic atomic pressure p_n written as

$$\sigma_n = \frac{1}{3}\sum_{i=1}^{3} \sigma_{ii} = -p_n = \frac{1}{3}\frac{dE_n(r_{nm})}{dr_{nm}} r_{nm}. \tag{4}$$

Dynamical properties are described by canonical molecular dynamics at constant temperature. The phonon energy exchange between adsorbate and substrate is ensured by the Andersen thermostat[51] involving stochastic collisions at the interface that simulate the cluster-surface phonon coupling. The MgO surface plays the role of the heat bath at a specific temperature. The system being in a vacuum, cluster surface atoms do not exchange heat with an external medium but with the oxide substrate. Such a technique has already been used in the melting of Pd nanoclusters on MgO(100) surface.[52]

B. Analytical expression of stress distribution due to periodic misfit interfacial dislocation given by the theory of elasticity

It is interesting to compare the atomistic numerical results with the analytical predictions given by the classical theory of elasticity. Various frameworks adequate for a description of interfacial misfit dislocations and their effects on the strain in a finite-thickness film have already been reported in the past.[38–40] Notably Bonnet and Verger-Gaugry[38] gave the general expressions of the stress field associated with a thin film epitaxially deposited on a substrate with regularly spaced misfit dislocations at the interface. It takes into account the lattice mismatch and different elastic constants for the two materials. However, such an expression is rather complex and requires a numerical resolution. It can be greatly simplified in the case of equal elastic constants of the substrate and the film, as proposed by Bourret.[39] In the case of a single direction dislocations system, parallel to the y axis ($\langle 110 \rangle$ direction in our system), the stress distribution is y independent and the only nonzero stress components at the surface are σ_{11}^I and $\sigma_{33}^I = \nu\sigma_{11}^I$. Using the dimensionless coordinates $X = 2\pi x/\Lambda$, $Z = 2\pi z/\Lambda$, and $H = 2\pi h/\Lambda$, with z perpendicular to the surface, the stress field is written as:[39]

$$\sigma_{11}^I(X,Z) = \frac{\mu f}{(1-\nu)}\sum_{n=1}^{\infty} \exp[-n(2H+Z)]\cos(nX) \times \{(nZ-2)\exp(2nH) + [n(2nH-1)Z - 2(nH-1)^2]\exp(2nZ)\}. \tag{5}$$

Taking into account the analytical form for the different summations:

$$S_1(X,H) = \sum_{n=1}^{\infty} \exp(-nH)\cos(nX) = -\frac{\cos(X) - \cosh(H) + \sinh(H)}{2[\cos(X) - \cosh(H)]}, \tag{6}$$

$$S_2(X,H) = \sum_{n=1}^{\infty} n \exp(-nH)\cos(nX) = \frac{-1+\cos(X)\cosh(H)}{2[\cos(X)-\cosh(H)]^2}, \tag{7}$$

$$S_3(X,H) = \sum_{n=1}^{\infty} n^2 \exp(-nH)\cos(nX) = \sinh(H)\frac{2-\cos(X)[\cos(X)+\cosh(H)]}{2[\cos(X)-\cosh(H)]^3}, \tag{8}$$

we obtain the analytical form:

$$\sigma_{11}^I(X,Z) = \frac{\mu f}{(1-\nu)}\{-2S_1(X,Z) + ZS_2(X,Z) - 2S_1(X,2H-Z) + (4H-Z)S_2(X,2H-Z) + 2H(Z-H)S_3(X,2H-Z)\}, \tag{9}$$

where μ and ν are, respectively, the shear modulus and Poisson ratio (μ=28 GPa and ν=0.37 for Ag) and $f=(a_{MgO}-a_{Ag})/a_{Ag}$=0.03. At the surface, $Z=H$ and expression (9) can be simplified as follows:

$$\sigma_{11}^I(X,H) = \frac{2f\mu}{(1-\nu)[\cos(X)-\cosh(H)]^2} \times \{H[\cos(X)\cosh(H) - 1] + [\cos(X)-\cosh(H)][\cos(X)-\cosh(H) + \sinh(H)]\} \tag{10}$$

Moreover, in the particular case of the surface, we can evaluate the complete stress in 2D dislocation arrays (x and y directions), which is given by the relations:

$$\sigma_{11}(X,Y,H) = \sigma_{11}^I(X,H) + \nu\sigma_{11}^I(Y,H),$$

$$\sigma_{33}(X,Y,H) = \sigma_{11}^I(Y,H) + \nu\sigma_{11}^I(X,H). \tag{11}$$

Along the diagonal of the pattern we have $X=Y$ so that the complete stress at the surface writes: $\sigma_{surf}=2(1+\nu)\sigma_{11}^I(X=Y,H)$ and is quantitatively comparable to the one calculated by numerical simulation as given in Eq. (4).

We will calculate, in the following, σ_{surf} and the amplitude of the stress modulation across the film $\Delta\sigma_{11}^I = |\sigma_{11}^I(0,Z) - \sigma_{11}^I(\pi,Z)|$ between the two extrema located on top of the dislocation core and in between. Finally, it is worth noting that as the free-standing layer is chosen as the reference lattice, there is no residual uniform misfit stress in the film, as compared to numerical simulation results where the periodicity of the simulation box imposes uniform strain in the Ag film.

III. ATOMIC STRUCTURE OF THE Ag LAYER ON MgO(100)

The semiempirical energetic model described before enables one to go beyond the model interfaces in perfect pseudomorphy as described by first-principle methods. When the system displays a lattice mismatch (such as Ag and MgO with 3%) the pseudomorphy imposes to dilate the Ag deposit in order to adopt the same lattice parameter than the MgO(100). In realistic epitaxial conditions, at the beginning of the growth, small clusters are partially strained as observed by high-resolution transmission electron microscopy on Pd clusters on MgO(100) (Ref. 53) or by x-ray absorption spectroscopy on Ag clusters on MgO(100),[37] and confirmed theoretically by our model.[41] Beyond a critical size, the elastic stress is released[50] via the introduction of misfit interfacial dislocations. These dislocations form a square network observed by GISAXS (Ref. 54) with a periodicity related to the misfit. The same result has been found for the Ag/MgO(100) system.[1,33,35] The end of the coalescence of the 3D clusters takes place above 30 ML and the interfacial edge dislocations oriented along the ⟨110⟩ direction reorganize into an ordered network with a period of about 9.7 nm (Ref. 33) to 10.95 nm (Ref. 1) depending on the preparation mode and on particular annealing conditions (higher temperature in the second case).

Although the larger part of the misfit induced stress (around 90%), if compared to pseudomorphy, is released by the introduction of interfacial dislocations, there is a residual stress associated with the dislocations cores that propagates across the film from the interface up to the free silver surface. This has been described in the framework of elasticity theory by Bonnet and Verger-Gaugry[38] and observed experimentally notably by GIXS on Si.[55] We propose here an atomistic description issued from quenched molecular dynamics simulation that allows one to describe, in detail, all of the atomic displacements, even in the core dislocations, going beyond the classic elastic theory. By comparing the results of the two kind of approaches, we get a nice qualitative agreement. We will see that they converge quantitatively at a sufficiently large distance from the core dislocation but differ sensibly in the vicinity of the lattice defect.

A. Effective misfit induced by thin-film effect

By quenched molecular simulations, we determined the minimum energy structure of a Ag film of 5 to 40 monolayers thickness. We found that the optimized periodicity (Λ) of the buried dislocation network changes significantly with the thickness of the film between 7 and 10 nm (i.e., 26 to 34 rows of silver atoms) as can be seen in Fig. 2. The energy differences are small (less than 1 meV) since they are related to a very small variation in the atomic positions. However, the variation of the dislocation network lattice, as a function of the film thickness, is relevant for an effective misfit effect related to the modification of the lattice parameter of the free thin silver film itself. Indeed, the optimized atomic structure of a free thin silver film with less than 40 monolayers shows a lateral lattice contraction of 1 to 2% so that the effective parameter of a film of 10 monolayers is only 4.05 Å instead of 4.09 Å in the bulk (value reached for the 40 monolayers thickness). The fact that the Ag–MgO(100) interaction is weak makes this finite-size effect more pronounced. It would disappear in the case of stronger interaction between the deposit and the support. It is important to notice however that these optimizations are performed at 0 K and could be influenced by thermic dilation at finite temperature. In the follow-

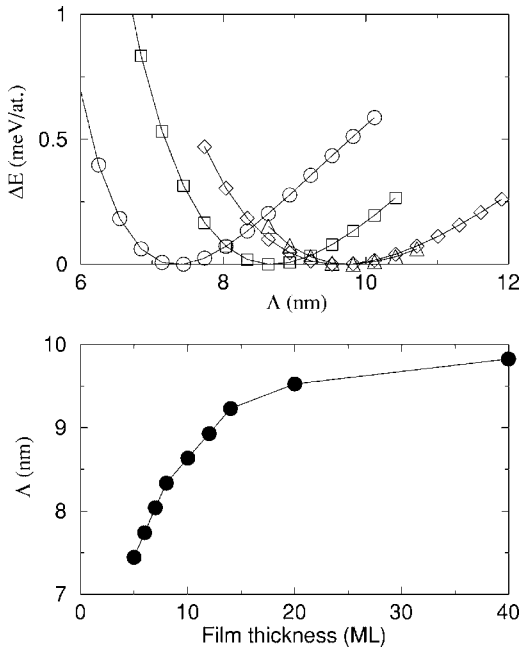

FIG. 2. Top graph: Average energy per atom as a function of the lateral periodicity Λ of the misfit dislocation network for different film thicknesses: 5 (circles), 10 (squares), 20 (diamonds), and 40 monolayer (triangles) . ΔE represents the energy difference with respect to the minimum. Bottom graph: Calculated evolution of the periodicity Λ as a function of the Ag film thickness.

ing, we will see the effect of the temperature on the structure of the film.

B. Stress distribution profile across a 34 monolayers silver film on MgO(100)

The stress distribution across a film of 34 Ag monolayers is displayed in Fig. 3. The stress profile of a cross-section of the film [Fig. 3(a)] is qualitatively similar to the one described by the elastic theory.[39] In the vicinity of the interface, we can distinguish a compressive (negative stress) zone on top of the misfit dislocations crossing (middle of the picture). The tensile (positive stress) zones are located at the border, between the dislocation cores. Around these areas, the stress is equal to the residual uniform stress per monolayer, i.e., less than 0.2% of GPa except at the surface and interface, where it is respectively 4.96 and 4.65 GPa, because of the metal bonds breaking. In Figs. 3(b)–3(e), we have plotted the modulation of the stress, plane by plane (perpendicular to the interface), to give a more precise view of the stress pattern and its evolution across the film. We can clearly see the central compressive zone (on top of the dislocations crossing) which is bounded by neutral zones and tensile zones on the corners. Then, moving from the interface toward the surface [from Figs. 3(b)–3(e)], we notice that the compressive area increases at the expense of the tensile ones. At the 28th layer, it splits into four compressive areas in the corners, driving to the opposite pattern as compared to the interfacial plane. This propagation of the stress and the pattern reversal are very comparable to that obtained in the framework of the

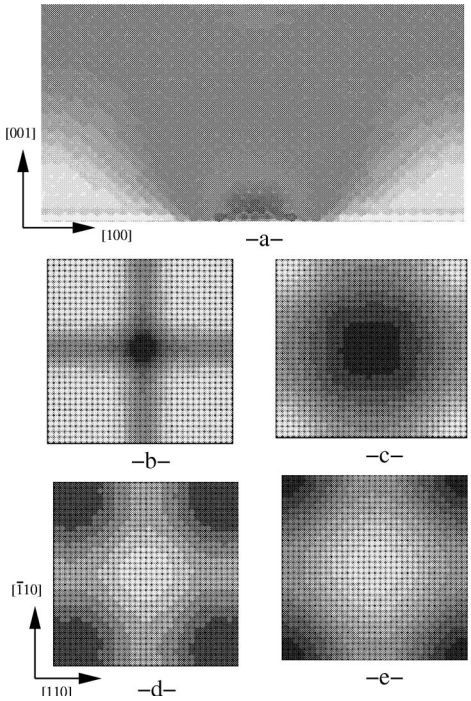

FIG. 3. (a) Atomic stress map in the cross section of the silver film perpendicular to the [010] direction for a $(34\times34\times34)$ Ag structure ($\Lambda=9.82$ nm). The dark zones correspond to sites in compression (negative stress), whereas bright ones correspond to sites in tension (positive stress). The atomic stress map is displayed also layer by layer: (b)–(e), respectively, for the 1st, 24th, 28th, and for the 34th (surface layer) perpendicular to the [001] direction to illustrate the inversion of compressive/tensile zones between the Ag-MgO interface and the Ag surface.

elasticity theory.[39] We can conclude here that from a qualitative point of view, the elasticity theory gives a good estimation of the stress propagation in the vicinity of misfit interfacial dislocation even if such a theory is *a priori* only valid at sufficient long-range distance. In the following, we will focus on thinner films and quantitatively compare the two approaches.

C. Surface patterning of the Ag/MgO(100) structure as a function of the Ag film thickness

We just have seen that the propagation of the stress perpendicularly to the interface leads to an inversion of the tensile and compressive areas near the surface. Now, we can ask if such a profile is conserved at the surface for Ag deposits of different thicknesses. The surface patterns of silver films of 5, 7, and 20 monolayers are displayed in Fig. 4. As mentioned before, the stress at the surface is strongly in tension due to the lack of bonds in the direction perpendicular to the surface. Its mean value has been suppressed in order to keep only the lateral modulations of the surface stress. The 20 monolayers deposit presents a surface pattern which remains essentially the same also for thicker deposits. As compared to the 34 monolayers deposit, the main variation consists of an additional extension of the tensile zone in the center [Fig. 3(e)]. It is accompanied by an increase of the surface stress

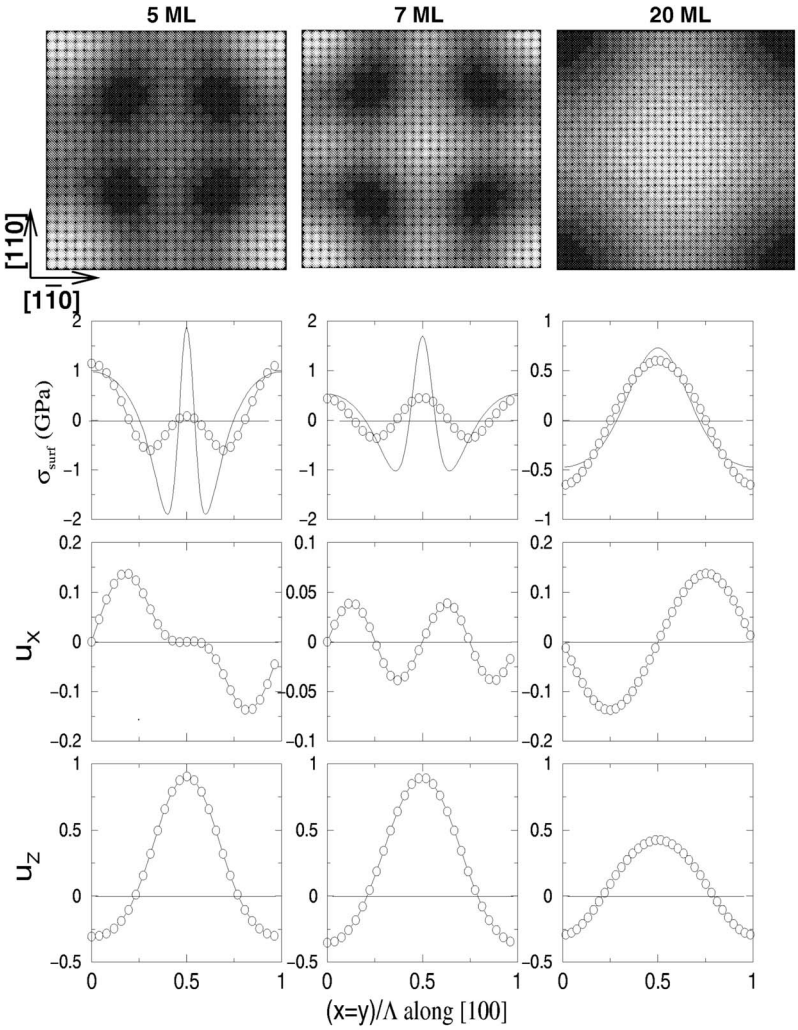

FIG. 4. Top panel represents the map of the surface atomic stress (same color code as in Fig. 3) for different film thicknesses: 5, 7, and 20 monolayers (1st, 2nd, and 3rd column, respectively). Bottom panel gives the corresponding atomic surface stress σ_{surf}(GPa) and displacements, parallel (u_x) and perpendicular (u_z) to the surface (Å), calculated along the [100] direction ($x=y$). Circles represent the atomistic calculations whereas full lines represent the elastic theory calculations.

amplitude, as will be seen in the following. Below 20 monolayers, the pattern design changes. Starting from the interface, where the compressive zones are located on top of the dislocation cores and tensile zones at the corners of the motif [see Fig. 3(b), the 5 monolayers deposit represents a small extension of this pattern, but with the separation of the central compressive zone and the emergence of a tensile zone in the middle of it (see Fig. 4 for 5 monolayers). The corresponding stress curve along the diagonal of the pattern ([100] direction) shows a small bump in its middle. By increasing the thickness of the deposit, the central zone extends and changes sign to form a periodicity which is one-half of the Λ one (see Fig. 4 for 7 monolayers). Then, the tensile zone in the center increases driving to the inversed pattern as observed in thicker films.

As compared to elasticity theory results, we notice a nice qualitative agreement: We observe the same inversion of the surface pattern as the thickness increases and for thin films, there is a periodic pattern with periodicity $\Lambda/2$. We find a quantitative agreement for the thicker films (20 monolayers) and far from the dislocation core ($x=0$ or $x=\Lambda$) in the thin films (5 and 7 monolayers). The main difference between the two approaches concerns the thinnest films in the direct vicinity of the dislocation core. The central zone under tension is much more localized and of larger amplitude in the elastic model than in the atomistic one (see the maximum of σ_{surf} at $x/\Lambda=0.5$ for the 5 and 7 monolayers films). Not surprisingly, the elasticity theory overestimates the stress in that region whereas the atomistic model is certainly more reliable in the description of the atomic structure of the dislocation core.

D. Evolution of the stress modulation across the film as a function of film thickness

We now focus on the variations of the stress modulation across films of different thicknesses. The amplitude modulations for different film thicknesses are reported in Fig. 5. The stress profile is oscillating in the vicinity of the interface and of the surface. This effect corresponds to a typical relaxation profile characteristic of metallic surfaces,[43] and is not accounted for by the elastic model. We notice also that the maximum of the modulation amplitude is reached in the first silver plane in contact with the MgO substrate, then, after small oscillations, it reaches a monotonic regime where it is

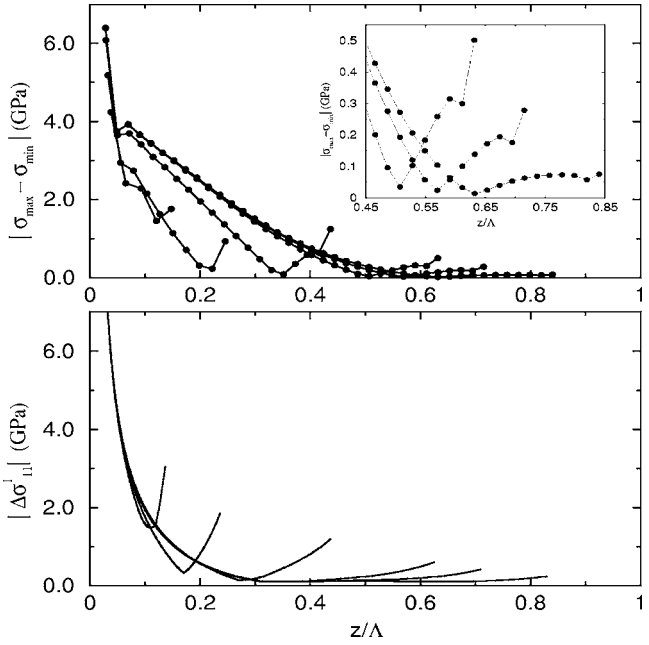

FIG. 5. Stress amplitude modulation across Ag films : $\Delta\sigma_{surf}=|\sigma_{max}-\sigma_{min}|$ obtained in the atomistic model (upper graph) and the same, expressed as $|\Delta\sigma^{I}_{11}|$ within the elasticity theory (lower graph) across Ag films of different thicknesses: 5, 10, 20, 30, 35, and 40 monolayer. The 30, 34, and 40 monolayer are zoomed in the insert.

damped before to be reinforced at the vicinity of the surface. The behavior of the stress amplitude is well reproduced by the elasticity theory, except the small oscillations near the interface. The minimum of $\Delta\sigma$, for films thicker than 10 monolayers, corresponds to the inversion of the pattern between interface and surface as detailed before. If the general behavior is similar in the two approaches, there are some clear differences in the vicinity of the interface. In the elastic model, the amplitude has the tendency to diverge (as $1/h$), whereas it is clearly delimited in the atomistic approach. This is a consequence of the localized character of tension zones on top of the dislocation core produced in the elasticity treatment, as shown before.

In Fig. 6, we have plotted the surface stress as a function of the thickness h/Λ for the two approaches, as well as the fits for $h \ll H$ in $1/h$ and for $h > \Lambda$ in $h\exp(h)$ (the exponential already fits the curve for $h/\Lambda > 0.5$). Once more, we can see that the two models give similar results for thick films (following the exponential behavior), but there is a clear discrepancy for thin films. In the intermediate region, the atomistic model displays a remarkable bump in order to link the two different regimes which is much more smooth in the elastic model. However, from $h/\Lambda = 0.4$ (20 monolayers), there is a remarkable agreement between the two different approaches.

E. Finite temperature results

Some simulations have been performed at finite temperature, in canonical ensemble, in order to check the stability of the structures described above. By performing molecular dynamics from 500 K to 700 K, a structure has emerged. It

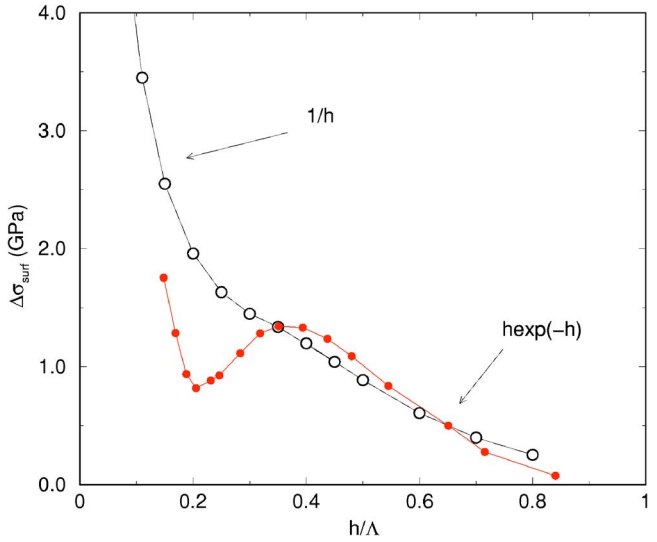

FIG. 6. (Color online) Stress amplitude modulation at the Ag film surface as a function of the film thickness (h/Λ): Atomistic model (full circles) and elasticity theory (empty circles). Regions corresponding to short-range ($1/h$) and long-range [$h\exp(-h)$] behavior are indicated.

presents (111) stacking faults induced by two sliding (111) planes forming a prismatic structure (illustrated in Fig. 7), as already obtained on Pd nanoclusters using a similar model.[41] This mechanism of strain relief has also been observed on a metallic heterostructure of Cu/Ni(100) by Müller *et al.*[56] who called it "internal (111) faceting". Constant temperature simulations show that such a structure is systematically obtained in one or two directions and is stable in a quite large temperature range (before the surface disordering). By quenching it, we can compare its internal energy with that of structures described before, and we find it systematically by about 1 meV/atoms lower. Taking into account the approximations of our model, notably the weak stacking fault energy in the metal (around 0.5 meV/atoms), a more detailed comparison with experimental results would be welcome.

IV. COBALT ADSORPTION ON THE PATTERNED Ag/MgO(100) SUBSTRATE

There has recently been some experimental evidence of self-organization of Co clusters on the Ag/MgO(100) patterned substrate[1] by *in situ* GISAXS. The buried dislocation network consisted of a 5 nm-thick Ag film (about 25 ML) on a MgO(100) substrate.

We have calculated the variations of the adsorption energy of one atomic Co along the [100] direction of the patterned silver surface for different film thicknesses. The adsorption energy is defined as :

$$E^{Co}_{ads} = E^{Co}_{Ag/MgO} - E_{Ag/MgO} - E^{Co}_{at}, \qquad (12)$$

where $E^{Co}_{Ag/MgO}$ and $E_{Ag/MgO}$ are the total energies of one Co atom on the Ag/MgO(100) substrate and the substrate alone. E^{Co}_{at} is the atomic energy of a Co atom in gas phase (chemical potential) equal to zero in our model. The Co–Ag interaction

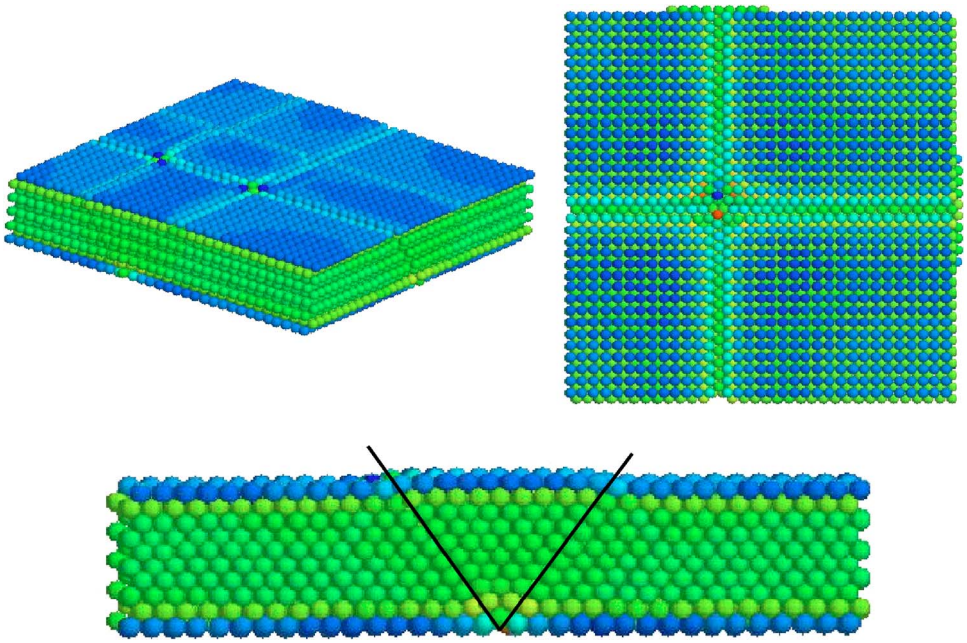

FIG. 7. (Color online) Internal (111) faceting structure for a 10 monolayer thick Ag film on MgO(100) substrate: Top view (Ag surface), bottom view (Ag interfacial plane), and side view.

is described within the SMA potential (Sec. II). The ξ and A parameters are fitted to the solubility energies of one Co impurity inside a silver bulk and *vice versa*. As the lattice parameters of the two metals differ by 13%, the fitting procedure takes into account the atomic relaxations around the impurity. The q and p parameters are simple averages of the corresponding parameters of pure elements. The values are given in Table I.

We have verified, using *ab initio* calculations within the DFT and the GGA, the adsorption energy of one Co atom on the perfect Ag(100) surface. Namely, using the VASP code[57] with the ultrasoft Vanderbilt pseudo-potentials[58] and a plane wave basis set, and taking into account the spin polarization, we found $E_{\mathrm{ads}}^{\mathrm{Co}}=-3.18$ eV, as compared to −3.27 eV given by the SMA potential.

It is worth noting that surface substitution can be in concurrence with adsorption on this surface. Surface substitution consists of substituting one Ag surface atom by the Co atom, and putting the Ag atom in adatom with the same expression as for the adsorption energy. In the SMA model, the surface substitution is nearly the same (surface adsorption is 10 meV more favorable than substitution). Unlike the adsorption, the substitution is much more sensitive to the atomic relaxation around the impurity. This can be seen by comparing the unreleased energy of the two systems adsorption/substitution within the SMA model: The substitution is lower in energy by about 200 meV, whereas at the end of the relaxation, the difference is about 10 meV in favor of the adsorption. As a consequence, the use of too small a box size in *ab initio* calculations can lead to the wrong result. We have performed the calculations for a box of variable sizes: Nine atoms by layer, and three or five layers. The results are, respectively, −3.57 eV and −3.13 eV so that with the larger box, the result is qualitatively in agreement with the SMA model favoring the adsorption energy by 50 meV (compared to 10 meV in SMA).

Results of the adsorption of one Co atom on the patterned Ag/Mg0(100) substrate of different silver thicknesses are illustrated in Fig. 8. We can notice that the adsorption is systematically favored on top of sites under tension, with laterally dilated interatomic distances. This is in nice agreement with *ab initio* calculations of Co adsorption on strained Pt(111) surface.[59] We further notice that the adsorption curve accurately follows the stress curve so that the surface stress is the driving force in the Co adsorption.

The present picture is considerably more simple than the adsorption of Co on the gold reconstructed (111) surface.[60]

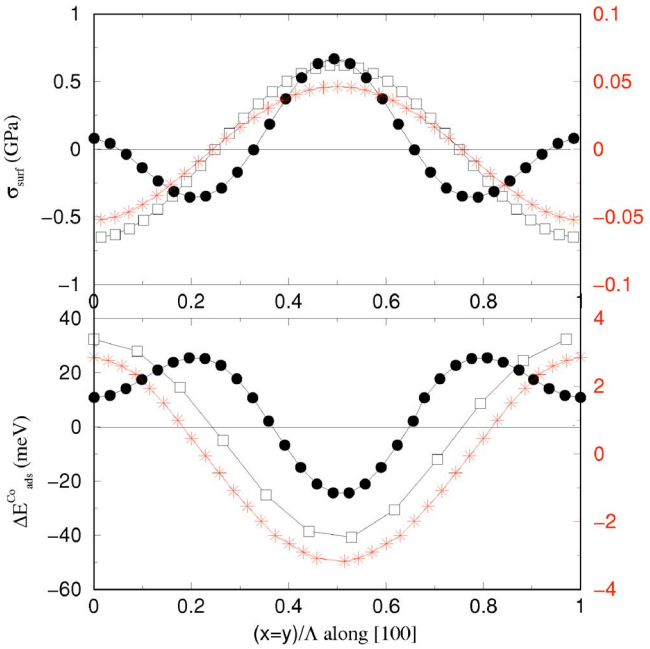

FIG. 8. (Color online) Surface stress (upper graph) and Co adsorption energy ($\Delta E_{\mathrm{ads}}^{\mathrm{Co}}$ being the difference between the adsorption energy on the Ag/MgO(100) patterned substrate and on the perfect Ag(100) surface] (lower graph), for different Ag thicknesses: 7 (full circles), 20 (empty squares), and 40 monolayers (stars with the verical scale on the right).

In that case, the adsorption is driven by the local surface relaxation, and the gold segregation tendency which creates pseudo-bridge sites with an effective four-fold coordination instead of the three-fold one expected on the (111) surface. However, the two systems Co/Au and Co/Ag display the same tendency to Au or Ag surface segregation, so that Co atom can easily be incorporated in the bulk. The preferential position is the subsurface site where the smaller atomic radius of the Co (as compared to Au or Ag) releases the strain in the subsurface. This region is usually compressed because of surface relaxation.

In the case of substitution of a surface Ag atom by Co, in the nanostructured silver film, the tendency is the opposite of the adsorption. The Co atom being smaller, it prefers to incorporate in sites under compression as to relax locally the stress. In the 20 monolayer film, taking the definition of the energy balance as in Fig. 8, we find $\Delta E_{\mathrm{subs}}^{\mathrm{Co}}=-40$ meV for $x/\Lambda=0$ and $\Delta E_{\mathrm{subs}}^{\mathrm{Co}}=20$ meV for $x/\Lambda=0.5$.

In order to bridge our results to the experimentally observed self-organization of Co clusters on the nanostructured Ag surface,[1] we have to make the assumption that the first adatom adsorption (or substitution) determines the position of nucleation center for the following cluster growth. Such a hypothesis has been confirmed by kinetic Monte Carlo simulations on Co self-organization on periodically strained Pt(111) surfaces.[59] As a consequence, also in the present case, the Co preferential adsorption/substitution sites may determine the Co cluster network. For Ag films thicker than 20 ML, the Co network will have the periodicity given by the Ag–MgO misfit. For the 7 to 10 monolayer Ag films, we may expect to obtain a Co cluster network periodicity two times smaller. But this has not been observed up until now. The comparison between the model and the experiments requires also that the roughness of the interface should be rather low (large surface terraces) and no impurity which can be achieved in real time *in situ* GISAXS experiments as performed by Leroy *et al.*[1]

Our assumption, that the cluster nucleation is controlled by the adsorption (or substitution) of the first adatom, disagrees partially with the elasticity theory. In fact, the elastic model predicts the nucleation rather in the region of compressive stress (in the middle of the dislocation squares).[39] This result is related to the misfit between the island and the substrate: In the case of $a_{\mathrm{island}}<a_{\mathrm{layer}}$, it is expected that the cluster prefers zones where interatomic distances are contracted in order to minimize the elastic strain in the island. This may signify that whereas adsorption of the first few atoms is indeed determined by E_{ads}, it is not necessarily the good criterion for a larger cluster. This raises the problem of kinetic effects (with nucleation and growth) compared to thermodynamic equilibrium driven by the minimization of elastic strain inside the island. These questions go beyond the scope of the present study and works are currently in progress in that direction.

V. CONCLUSIONS

The characterization of an heteroepitaxial silver film on MgO(100) substrate with buried misfit interfacial dislocations has been performed by atomistic simulations and compared to the predictions of the elasticity theory. The agreement is satisfying on sufficiently thick films (>20 monolayers), and partially good for thin films of less than 10 monolayers. Surprisingly, for these thin films, we still get reasonably good agreement far from the dislocation core (at the center of the dislocations network). In the vicinity of the dislocation cores, the elasticity theory comes to its limits of validity and the atomistic simulation gives a more realistic picture of the structure. The calculated adsorption (respectively substitution) energy of Co atoms on the nanostructured Ag surface shows a preferential adsorption on top of zones under tensile (respectively compressive) stress. This could be a first indication of stress-driving self-organization on this surface. Works are still in progress in that direction to better describe the self-organization process.

ACKNOWLEDGMENTS

A. O. thanks the CROUS of the University of Aix-Marseille for his grant. We acknowledge financial support from the European Commission for the project STREP-GSOMEN. The CRMCN is associated with the Universities of Aix-Marseille II and III.

*Author to whom correspondence should be addressed; electronic mail: mottet@crmcn.univ-mrs.fr

[1] F. Leroy, G. Renaud, A. Letoublon, R. Lazzari, C. Mottet, and J. Goniakowski (unpublished).

[2] J. M. Moison, F. Houzay, F. Barthe, L. Leprince, E. Andr, and O. Vatel, Appl. Phys. Lett. **64**, 196 (1994).

[3] O. Fruchart, M. Klaua, J. Barthel, and J. Kirschner, Phys. Rev. Lett. **83**, 2769 (1999).

[4] S. Degen, C. Becker, and K. Wandelt, Faraday Discuss. **125**, 343 (2004).

[5] K. Pohl, M. C. Bartelt, J. de la Figuera, N. C. Bartelt, J. Hrbek, and R. Q. Hwang, Nature (London) **397**, 238 (1999).

[6] D. D. Chambliss, R. J. Wilson, and S. Chiang, Phys. Rev. Lett. **66**, 1721 (1991).

[7] B. Voigtlander, G. Meyer, and N. M. Amer, Phys. Rev. B **44**, 10354 (1991).

[8] F. Besenbacher, L. P. Nielsen, and P. T. Sprunger, in *Growth and Properties of Ultrathin Epitaxial Layers*, edited by D. A. King and D. P. Woodruff (Elsevier, Amsterdam, 1997), Vol. 8, p. 207.

[9] H. Brune and K. Kern, in *Growth and Properties of Ultrathin Epitaxial Layers*, edited by D. A. King and D. P. Woodraff (Elsevier, Amsterdam, 1997), Vol. 8, p. 149.

[10] B. Croset, Y. Girard, G. Prévot, M. Sotto, Y. Garreau, R. Pinchaux, and M. Sauvage-Simkin, Phys. Rev. Lett. **88**, 056103 (2002).

[11] C. Mottet, G. Tréglia, and B. Legrand, Phys. Rev. B **46**, 16018

(1992).
[12] H. Brune, H. Roder, C. Boragno, and K. Kern, Phys. Rev. B **49** R2997 (1994).
[13] J. Jacobsen, L. P. Nielsen, F. Besenbacher, I. Stensgaard, E. Laegsgaard, T. Rasmussen, K. W. Jacobsen, and J. K. Norskov, Phys. Rev. Lett. **75**, 489 (1995).
[14] B. Aufray, M. Göthelid, J.-M. Gay, C. Mottet, E. Landemark, G. Falkenberg, L. Lottermoser, L. Seehofer, and R. L. Johnson, Microsc. Microanal. Microstruct. **8**, 167 (1997).
[15] I. Meunier, G. Tréglia, J.-M. Gay, B. Aufray, and B. Legrand, Phys. Rev. B **59**, 10910 (1999).
[16] H. Brune, M. Giovannini, K. Bromann, and K. Kern, Nature (London) **394**, 451 (1998).
[17] K. Bromann, M. Giovani, H. Brune, and K. Kern, Eur. Phys. J. D **9**, 25 (1999).
[18] Y. H. Xie, S. B. Samavedam, M. Bulsara, T. A. Langdo, and E. A. Fitzgerald, Appl. Phys. Lett. **71**, 3567 (1997).
[19] S. Y. Shiryaev, F. Jensen, J. L. Hansen, J. W. Petersen, and A. N. Larsen, Phys. Rev. Lett. **78**, 503 (1997).
[20] W. P. Vellinga, J. T. M. De Hosson, and V. Vitek, Acta Mater. **45**, 1525 (1997).
[21] M. W. Finnis, A. M. Stoneham, P. W. Tasker, *Metal-Ceramic Interfaces*, Acta Scripta Metall. Proceedings Series Vol. 4 (Pergamon, New York, 1990).
[22] V. E. Henrich and P. A. Cox, *The Surface Science of Metal Oxides* (Cambridge University Press, Cambridge, UK, 1996).
[23] L. Spiess, Surf. Rev. Lett. **3**, 1365 (1996).
[24] E. Heifets, Y. F. Zhukovskii, E. A. Kotomin, and M. Causa, Chem. Phys. Lett. **283**, 395 (1998).
[25] J. A. Purton, D. M. Bird, S. C. Parker, and D. W. Bullett, J. Chem. Phys. **110**, 8090 (1999).
[26] D. Fuks, S. Dorfman, E. A. Kotomin, Y. F. Zhukovskii, and A. M. Stoneham, Phys. Rev. Lett. **85**, 4333 (2000).
[27] Y. F. Zhukovskii, E. A. Kotomin, P. W. M. Jacobs, and A. M. Stoneham, Phys. Rev. Lett. **84**, 1256 (2000); Y. F. Zhukovskii, E. A. Kotomin, D. Fuks, S. Dorfman, and A. Gordon, Surf. Sci. **482**, 66 (2001); Y. F. Zhukovskii, E. A. Kotomin, and G. Borstel, Vacuum **74**, 235 (2004).
[28] G. Pacchioni, Surf. Sci. **520**, 3 (2002).
[29] R. Benedek, D. N. Seidman, and C. Woodward, J. Phys.: Condens. Matter **14**, 2877 (2002).
[30] S. Mogck, B. J. Kooi, J. Th. M. De Hosson, and M. W. Finnis, Phys. Rev. B **70**, 245427 (2004).
[31] A. Trampert, F. Ernst, C. P. Flynn, H. F. Fischmeister, and M. Rühle, Acta Metall. Mater. **40**, S227 (1992).
[32] A. M. Flank, R. Delaunay, P. Lagarde, M. Pompa, and J. Jupille, Phys. Rev. B **53**, R1737 (1996).
[33] G. Renaud, P. Guénard, and A. Barbier, Phys. Rev. B **58**, 7310 (1998).
[34] O. Robach, G. Renaud, and A. Barbier, Surf. Sci. **401**, 227 (1998).
[35] O. Robach, G. Renaud, and A. Barbier, Phys. Rev. B **60**, 5858 (1999).
[36] H. B. Groen, B. J. Kooi, W. P. Vellinga, and J. T. M. Dehosson, Philos. Mag. A **79**, 2083 (1999).
[37] P. Lagarde, S. Colonna, A.-M. Flank, and J. Jupille, Surf. Sci. **524**, 102 (2003).
[38] R. Bonnet and J. L. Verger-Gaugry, Philos. Mag. A **66**, 849 (1992).
[39] A. Bourret, Surf. Sci. **432**, 37 (1999).
[40] J. R. Willis, S. C. Jain, and R. Bullough, Philos. Mag. A **62**, 115 (1990).
[41] W. Vervisch, C. Mottet, and J. Goniakowski, Phys. Rev. B **65**, 245411 (2002).
[42] J. Goniakowski, Phys. Rev. B **57**, 1935 (1998); **58**, 1189 (1998); **59**, 11047 (1999).
[43] V. Rosato, M. Guillopé, and B. Legrand, Philos. Mag. A **59**, 321 (1989).
[44] M. S. Daw, M. I. Baskes, Phys. Rev. Lett. **50**, 1285 (1983).
[45] J. Friedel, *The Physics of Metals*, edited by J. M. Ziman (Cambridge University Press, Cambridge, UK, 1969), p. 340.
[46] C. Kittel, *Introduction to Solid State Physics*, 7th ed. (Wiley, New York, 1996).
[47] G. Simmons and H. Wang, *Single Crystal Elastic Constants and Calculated Aggregated Properties* (MIT, Cambridge, MA, 1971).
[48] P. Blaha, K. Schwarz, and J. Luitz, WIEN97, Vienna University of Technology, 1997. [Improved and updated Unix version of the original copyrighted WIEN code, which was published by P. Blaha, K. Schwarz, P. Sorantin, and S. B. Trickey, in Comput. Phys. Commun. **59**, 399 (1990)].
[49] http://www.crmcn.univ-mrs.fr/gModel/webparam.pdf
[50] W. Vervisch, C. Mottet, and J. Goniakowski, Eur. Phys. J. D **24**, 311 (2003).
[51] H. C. Andersen, J. Chem. Phys. **72**, 2384 (1980).
[52] C. Mottet and J. Goniakowski, Surf. Sci. **566**, 443 (2004).
[53] H. Graoui, S. Giorgio, and C. R. Henry, Philos. Mag. B **81**, 1649 (2001).
[54] G. Renaud, A. Barbier, and O. Robach, Phys. Rev. B **60**, 5872 (1999).
[55] F. Leroy, J. Eymery, D. Buttard, G. Renaud, R. Lazzari, and F. Fournel, Appl. Phys. Lett. **82**, 2598 (2003).
[56] B. Müller, B. Fischer, L. Nedelmann, A. Fricke, and K. Kern, Phys. Rev. Lett. **76**, 2358 (1996).
[57] G. Kresse and J. Hafner, Phys. Rev. B **47**, R558 (1993); G. Kresse, thesis, Technische Universität, Wien, 1993; G. Kresse and J. Furthmüller, Phys. Rev. B **54**, 11169 (1996).
[58] D. Vanderbilt, Phys. Rev. B **32**, 8412 (1985).
[59] R. F. Sabiryanov, M. I. Larsson, K. Cho, W. D. Nix, and B. M. Clemens, Phys. Rev. B **67**, 125412 (2003).
[60] C. Goyhenex and H. Bulou, Phys. Rev. B **63**, 235404 (2001); C. Goyhenex, H. Bulou, J.-P. Deville, and G. Tréglia, Appl. Surf. Sci. **188**, 134 (2002).